Effective-Mass Theory of Electron Correlations in Band Structure of Semiconducting Carbon Nanotubes

Hideaki SAKAI, Hidekatsu SUZUURA[1] and Tsuneya ANDO[1]

Institute for Solid State Physics, University of Tokyo
5–1–5 Kashiwanoha, Kashiwa, Chiba 277-8581

[1] *Department of Physics, Tokyo Institute of Technology*
2–12–1 Ookayama, Meguro-ku, Tokyo 152-8551

The band gap, the single-particle energy, and the effective mass are calculated for semiconducting carbon nanotubes in a random-phase approximation within a $\boldsymbol{k}\cdot\boldsymbol{p}$ scheme. The energy gaps are shown to be strongly enhanced due to the Coulomb interaction, while effects on the effective mass along the axis direction are small. For realistic values of the interaction parameter, effects of the dynamical screening are sufficiently weak, and the conventional screened Hartree-Fock approximation is shown to work quite well. Further, the band gap contains a term with a residual logarithmic dependence on the tube diameter d after being scaled by $1/d$.

Keywords: graphite, carbon nanotube, electron-electron interaction, dynamical RPA, band gap, single-particle energy, effective-mass theory

§1. Introduction

A carbon nanotube (CN) was first discovered by Iijima in 1991.[1)] It consists of coaxially rolled two-dimensional (2D) graphite sheets and its electronic states change critically from metallic to semiconducting depending on its tubular circumferential vector. The characteristic properties were first predicted by the band-structure calculation in a tight-binding model[2−10)] and successfully reproduced in a $\boldsymbol{k}\cdot\boldsymbol{p}$ scheme or an effective-mass approximation.[11,12)] The purpose of this work is to study effects of the mutual Coulomb interaction on the band structure within such a $\boldsymbol{k}\cdot\boldsymbol{p}$ scheme.

Effects of the Coulomb interaction on the band structure were evaluated within a conventional screened Hartree-Fock approximation.[13)] The results show that the band gap is considerably enhanced by the Coulomb interaction. In this approximation the dielectric function appearing in the self-energy is replaced by the static one and therefore dynamical effects such as coupling with virtual charge density excitations are not taken into consideration. In this paper, we calculate the electronic states of semiconducting CN's using a full dynamical random-phase approximation (RPA), which is often called the GW approximation.[14)]

Experimentally, the one-dimensional electronic structure of a CN was directly observed by scanning tunneling microscopy and spectroscopy[15,16)] and the resonant Raman scattering.[17)] Optical absorption spectra of a single-wall nanotube also reflect its band structure,[18,19)] though excitonic effects can be important.[13,20,21)] For a better understanding of such experiments, it is certainly meaningful to make more precise evaluations of the electronic band structure with effects of the Coulomb interaction taken into account.

In this paper, we shall calculate the single-particle energy and the effective mass in semiconducting carbon nanotubes in a random-phase approximation within a $\boldsymbol{k}\cdot\boldsymbol{p}$ scheme. In §2, the self-energy is introduced and the method of its explicit calculation is described after a brief introduction on the effective-mass scheme. Numerical results are presented in §3 and discussed in §4. A short summary is given in §5.

§2. Electron-Electron Interaction

2.1 Effective-mass scheme

In the effective-mass approximation, electronic states of a 2D graphite near the K point are described by the $\boldsymbol{k}\cdot\boldsymbol{p}$ equation as[22,11)]

$$\gamma(\sigma\cdot\hat{\boldsymbol{k}})\boldsymbol{F}^K(\boldsymbol{r})=\varepsilon\boldsymbol{F}^K(\boldsymbol{r}), \tag{2.1}$$

with γ being the band parameter without interaction, $\sigma=(\sigma_x,\sigma_y)$ the Pauli spin matrices, and $\hat{\boldsymbol{k}}=(\hat{k}_x,\hat{k}_y)$ a wave vector operator. For a CN, its electronic states are obtained by imposing the boundary conditions in the circumference direction:[11)]

$$\boldsymbol{F}^K(\boldsymbol{r}+\boldsymbol{L})=\boldsymbol{F}^K(\boldsymbol{r})\exp\Big(-\frac{2\pi\mathrm{i}\nu}{3}\Big). \tag{2.2}$$

The integer ν is 0 or ±1, determined by $n_a+n_b=3M+\nu$ with integer M, where $\boldsymbol{L}=n_a\boldsymbol{a}+n_b\boldsymbol{b}$ is the chiral vector in the circumference direction and $\boldsymbol{a}$ and $\boldsymbol{b}$ are the primitive translation vectors of a 2D graphite.

Around the K point, the wave function and the energy bands are given by

$$\begin{aligned}\boldsymbol{F}^K_{nsk}(\boldsymbol{r})&=\frac{1}{\sqrt{AL}}\boldsymbol{F}^{\nu K}_{nsk}\exp\big[\mathrm{i}\kappa_\nu(n)x+\mathrm{i}ky\big],\\ \varepsilon^K_{ns}(k)&=s\gamma\sqrt{\kappa_\nu(n)^2+k^2},\end{aligned} \tag{2.3}$$

with

$$\begin{aligned}\boldsymbol{F}^{\nu K}_{nsk}&=\frac{1}{\sqrt{2}}\begin{pmatrix}b_\nu(n,k)\\ +s\end{pmatrix},\\ b_\nu(n,k)&=\frac{\kappa_\nu(n)-\mathrm{i}k}{\sqrt{\kappa_\nu(n)^2+k^2}},\\ \kappa_\nu(n)&=\frac{2\pi}{L}\Big(n-\frac{\nu}{3}\Big),\end{aligned} \tag{2.4}$$

where $L=|\boldsymbol{L}|$, A is the length of a CN, the x axis is chosen along the circumference direction, and the y axis

Submitted to Journal of Physical Society of Japan

is parallel to the tube axis. Further, n is an integer, k the wave vector in the axis direction, and s the band index ($s=+1$ for the conduction band and $s=-1$ for the valence band). Equations for the K' point are the same as those for the K point except that σ_y is replaced by $-\sigma_y$ and ν by $-\nu$.

2.2 Coulomb interaction

The Coulomb potential between two electrons on the cylindrical surface at $\boldsymbol{r}=(x,y)$ and $\boldsymbol{r}'=(x',y')$ is written as[23–27]

$$v(x-x',y-y') = \sum_q \exp\left[\mathrm{i}q(y-y')\right]\frac{2e^2}{\kappa A}K_0\Big(\frac{L|q|}{2\pi}\Big|2\sin\frac{\pi(x-x')}{L}\Big|\Big), \tag{2.5}$$

where $K_n(t)$ is the modified Bessel function of the second kind and κ is a static dielectric constant representing effects of the polarization of electrons in core states, filled σ bands, and also occupied π bands away from the K and K' points. In the effective-mass approximation, this potential appears only in the diagonal part of the matrix $\boldsymbol{k}\cdot\boldsymbol{p}$ Hamiltonian, and the Coulomb matrix elements are given by

$$\langle\alpha,k,K;\beta',k'+q,K|v|\beta,k+q,K;\alpha',k',K\rangle = \frac{1}{A}\delta_{n-m,n'-m'}\left(\boldsymbol{F}^{\nu K*}_{\alpha k}\cdot\boldsymbol{F}^{\nu K}_{\beta k+q}\right)\left(\boldsymbol{F}^{\nu K*}_{\beta' k'+q}\cdot\boldsymbol{F}^{\nu K}_{\alpha' k'}\right)v_{n-m}(q), \tag{2.6}$$

with

$$v_{n-m}(q) = \frac{2e^2}{\kappa}I_{|n-m|}\Big(\frac{L|q|}{2\pi}\Big)K_{|n-m|}\Big(\frac{L|q|}{2\pi}\Big), \tag{2.7}$$

where $I_n(t)$ is the modified Bessel function of the first kind and $\alpha=(n,\pm)$, $\beta=(m,\pm)$, etc. Note that matrix elements corresponding to the scattering of an electron from the K point to the K' point and vice versa are safely neglected in the effective-mass approximation.

In RPA, the Coulomb interaction is screened by the dynamical dielectric function $\varepsilon_{n-m}(q,\omega)$, given by

$$\varepsilon_{n-m}(q,\omega) = 1 + v_{n-m}(q)P_{n-m}(q,\omega). \tag{2.8}$$

The polarization function $P_{n-m}(q,\omega)$ is expressed as

$$P_{n-m}(q,\omega) = -\frac{2}{A}\sum_{G=K,K'}\sum_{n',m'}\sum_{k'}\delta_{n-m,n'-m'} \times F^{\nu G}_{m'+,k';n'-,k'+q}\,g_0[\varepsilon^G_{m'+}(k')]\,g_0[\varepsilon^G_{n'-}(k'+q)] \times\Big[\frac{1}{\omega-\varepsilon^G_{m'+}(k')+\varepsilon^G_{n'-}(k'+q)+\mathrm{i}\delta} - \frac{1}{\omega+\varepsilon^G_{m'+}(k')-\varepsilon^G_{n'-}(k'+q)-\mathrm{i}\delta}\Big], \tag{2.9}$$

with δ being a positive infinitesimal,

$$F^{\nu G}_{\alpha,k;\beta,k+q} = |\boldsymbol{F}^{\nu G*}_{\alpha,k}\cdot\boldsymbol{F}^{\nu G}_{\beta,k+q}|^2 = \frac{1}{2}\Big(1+\frac{s_\alpha s_\beta[\kappa_\nu(n)\kappa_\nu(m)+k(k+q)]}{\sqrt{\kappa_\nu(n)^2+k^2}\sqrt{\kappa_\nu(m)^2+(k+q)^2}}\Big), \tag{2.10}$$

and

$$s_\alpha = \begin{cases}+1 & (\alpha=n+),\\ -1 & (\alpha=n-),\end{cases} \tag{2.11}$$

where G takes the K and K' point. The cutoff function $g_0(\varepsilon)$ is given by

$$g_0(\varepsilon) = \frac{\varepsilon_c^{\alpha_c}}{|\varepsilon|^{\alpha_c}+\varepsilon_c^{\alpha_c}}, \tag{2.12}$$

which contains two parameters α_c and ε_c so as to take only the contributions from states in the vicinity of the Fermi level into consideration. The introduction of $g_0(\varepsilon)$ makes numerical calculations easy, but actually is not necessary in the polarization function because the summation in eq. (2.9) converges even for $\varepsilon_c\to\infty$. Obviously, the dielectric function satisfies

$$\varepsilon_{n-m}(q,\omega) = \varepsilon_{n-m}(q,-\omega). \tag{2.13}$$

2.3 Self-energy

Formally, the effective interaction gives the self-energy for electrons in the dynamical RPA including the cutoff function as

$$\tilde{\Sigma}^K_\alpha(k,\omega) = \frac{\mathrm{i}}{2\pi A}\int\mathrm{d}\omega'\sum_{\beta,q}G^K_\beta(k+q,\omega+\omega')F^{\nu K}_{\alpha,k;\beta,k+q} \times\frac{v_{n-m}(q)}{\varepsilon_{n-m}(q,\omega')}e^{\mathrm{i}\delta\omega'}g_0[\varepsilon^K_\beta(k+q)], \tag{2.14}$$

where $G^K_\alpha(k,\omega)$ is the non-interacting Green's function written as

$$G^K_\alpha(q,\omega) = \frac{1}{\omega-\varepsilon^K_\alpha(q)+\mathrm{i}s_\alpha\delta}. \tag{2.15}$$

Equation (2.14) is represented in terms of Feynman diagrams shown in Fig. 1.

The original $\boldsymbol{k}\cdot\boldsymbol{p}$ Hamiltonian has the particle-hole symmetry about $\varepsilon=0$. It leads to

$$G^K_{\bar\alpha}(q,-\omega) = -G^K_\alpha(q,\omega), \tag{2.16}$$

$$F^{\nu K}_{\alpha,k;\beta,k+q} = F^{\nu K}_{\bar\alpha,k;\bar\beta,k+q}, \tag{2.17}$$

where $\bar\alpha$ means a state with energy opposite to state α, i.e., $\bar\alpha=n-$ for $\alpha=n+$, $\bar\alpha=n+$ for $\alpha=n-$, etc. It should also lead to the symmetry of the band structure in the presence of interactions if the energy is measured from the Fermi level.

The self-energy can be separated into

$$\tilde{\Sigma}^K_\alpha(k,\omega) = \tilde{\Sigma}^K_\alpha(k,\omega)^{\mathrm{X}} + \tilde{\Sigma}^K_\alpha(k,\omega)^{\mathrm{C}}, \tag{2.18}$$

where the exchange or Hartree-Fock term $\tilde{\Sigma}^K_\alpha(k,\omega)^{\mathrm{X}}$ and the correlation term $\tilde{\Sigma}^K_\alpha(k,\omega)^{\mathrm{C}}$ are defined by

$$\tilde{\Sigma}^K_\alpha(k,\omega)^{\mathrm{X}} = \frac{\mathrm{i}}{2\pi A}\int\mathrm{d}\omega'\sum_{\beta,q}G^K_\beta(k+q,\omega+\omega')F^{\nu K}_{\alpha,k;\beta,k+q} \times v_{n-m}(q)\mathrm{e}^{\mathrm{i}\omega'\delta}g_0[\varepsilon^K_\beta(k+q)], \tag{2.19}$$

and

$$\tilde{\Sigma}^K_\alpha(k,\omega)^{\mathrm{C}} = \frac{\mathrm{i}}{2\pi A}\int\mathrm{d}\omega'\sum_{\beta,q}G^K_\beta(k+q,\omega+\omega')F^{\nu K}_{\alpha,k;\beta,k+q} \times v_{n-m}(q)\Big(\frac{1}{\varepsilon_{n-m}(q,\omega')}-1\Big)g_0[\varepsilon^K_\beta(k+q)], \tag{2.20}$$

respectively. Because the integrand of eq. (2.20) decays faster than $1/\omega'$ for large $|\omega'|$, the convergence factor

$e^{i\delta\omega'}$ has been omitted in the expression of the correlation part. Then, the symmetry relations (2.16) and (2.17) together with eq. (2.13) immediately lead to the electron-hole symmetry for the correlation part, i.e.,

$$\tilde{\Sigma}_{\bar{\alpha}}(k,-\omega)^{\mathrm{C}} = -\tilde{\Sigma}_{\alpha}(k,\omega)^{\mathrm{C}}. \tag{2.21}$$

On the other hand, the contribution from the Hartree-Fock term can be evaluated with ease by closing the contour for ω' in the upper-plane, giving the self-energy in the Hartree-Fock approximation:

$$\tilde{\Sigma}^K_{\alpha}(k)^{\mathrm{X}} = -\frac{1}{A}\sum_{m,q} F^{\nu K}_{\alpha,k;m-,k+q}\, v_{n-m}(q)\, g_0[\varepsilon^K_{m-}(k+q)], \tag{2.22}$$

which is independent of ω. With the use of eq. (2.10), we obtain

$$\begin{aligned}&\frac{1}{2}\big[\tilde{\Sigma}^K_{n+}(k)^{\mathrm{X}}+\tilde{\Sigma}^K_{n-}(k)^{\mathrm{X}}\big]\\ &= -\frac{1}{2A}\sum_{m,q} v_{n-m}(q)\, g_0\big(\gamma\sqrt{\kappa(m)^2+(k+q)^2}\big).\end{aligned} \tag{2.23}$$

The cutoff function is necessary in this average self-energy because it diverges in proportion to ε_c for $\varepsilon_c\to\infty$. As a result it has a small dependence on the band n and the wave vector k through the cutoff function, which violates the electron-hole symmetry although very slightly. In actual systems with finite band width where such a cutoff function is not necessary, this quantity represents a constant shift in the exchange energy independent of n and k and makes no contribution to the band gap or to the effective mass.

In the present effective-mass scheme, therefore, we should redefine the self-energy by subtracting this constant energy shift as

$$\Sigma^K_{n\pm}(k,\pm\omega) \equiv \pm\frac{1}{2}\big[\tilde{\Sigma}^K_{n+}(k,\omega) - \tilde{\Sigma}^K_{n-}(k,-\omega)\big], \tag{2.24}$$

with the upper sign in the right hand side corresponding to $\Sigma^K_{n+}(k,\omega)$ and the lower sign $\Sigma^K_{n-}(k,-\omega)$. We then obtain the particle-hole symmetric self-energy, i.e., $\Sigma^K_{n+}(k,\omega) = -\Sigma^K_{n-}(k,-\omega)$ even if the cutoff function is introduced.

When the frequency dependence of the dielectric function in eq. (2.14) is neglected and $\varepsilon_{n-m}(q,\omega)$ is replaced by $\varepsilon_{n-m}(q,0)$, the self-energy is reduced to that in the screened Hartree-Fock approximation, which has been used in a previous work.[13] This approximation can also be called the static RPA. The resulting self-energy is obtained by the replacement $v_{n-m}(q)$ by $v_{n-m}(q)\varepsilon_{n-m}(q,0)^{-1}$ in eq. (2.22). In the following, the results are compared with those obtained in such more simplified approximations as the static RPA and the Hartree-Fock approximation.

2.4 Single-particle energy, band gap, and effective mass

In this paper, the single-particle energy $E^K_n(k)$ around the K point is given by

$$E^K_{n\pm}(k) = \varepsilon^K_{n\pm}(k) + \Sigma^K_{n\pm}(k,\varepsilon^K_{n\pm}(k)). \tag{2.25}$$

Originally, the single-particle energy is determined by the equation obtained from the above by the replacement of $\Sigma^K_{n\pm}(k,\varepsilon^K_{n\pm}(k))$ by $\Sigma^K_{n\pm}(k,E^K_{n\pm}(k))$. However, eq. (2.25) is known to give more accurate results if the self-energy is calculated only in the lowest order as in the present case.[28,29]

Using the above singe-particle energy, we evaluate the band gap Δ^K_n which is defined by the energy difference at $k=0$ between conduction and valence bands of the same index n associated with the K point for a semiconducting CN ($\nu=1$) as

$$\Delta^K_n = E^K_{n+}(0) - E^K_{n-}(0), \tag{2.26}$$

The effective mass $m^{K*}_{n\pm}$ for each band with Coulomb interaction can also be estimated from the single-particle energy $E^K_{n\pm}(k)$, i.e.,

$$\frac{1}{m^{K*}_{n\pm}} = \frac{1}{\hbar^2}\frac{\partial^2 E^K_{n\pm}(k)}{\partial k^2}\Big|_{k=0}. \tag{2.27}$$

In general, the imaginary part of the self-energy comes solely from $\Sigma^K_{\alpha}(k,\omega)^{\mathrm{C}}$ in the dynamical RPA since $\Sigma^K_{\alpha}(k,\omega)^{\mathrm{X}}$ is real. In semiconducting CN's at zero temperature, however, the imaginary part of $\Sigma^K_{\alpha}(k,\varepsilon^K_{\alpha}(k))^{\mathrm{C}}$ is actually zero and the self-energy then has only the real part. This result reflects the fact that the momentum and energy conservation prevents a single particle-hole pair excitation in the present system with a gap.

§3. Results

3.1 Numerical calculations

The effective strength of the Coulomb interaction is specified by the ratio between the effective Coulomb energy $e^2/\kappa L$ and the typical kinetic energy $2\pi\gamma/L$, i.e., $(e^2/\kappa L)/(2\pi\gamma/L)$, which is independent of the circumference length L. In actual nanotubes, the interaction parameter is estimated as $(e^2/\kappa L)/(2\pi\gamma/L) = (e^2/\kappa a)/\gamma_0$ for $\gamma = \sqrt{3}a\gamma_0/2$ where $-\gamma_0$ is the transfer integral between the nearest neighbor carbon atoms in a simplest tight-binding model and a is the lattice constant.

For $\gamma_0 \sim 3$ eV and $a = 2.46$ Å, this gives $(e^2/\kappa L)/(2\pi\gamma/L) \sim 0.35/\kappa < 0.35$ because it is expected that $\kappa > 1$. In the following, however, we shall treat the above quantity as the interaction parameter and perform calculations for $0 < (e^2/\kappa L)/(2\pi\gamma/L) < 1$ in order to make the dependence on the interaction strength clear. The cutoff parameters are chosen as $\varepsilon_c/(2\pi\gamma/L)=5$ and $\alpha_c=4$ in most of the cases and the cutoff dependence is studied also.

Poles of $\varepsilon_{n-m}(q,\omega)^{-1}$ along the real axis make it quite difficult to calculate $\tilde{\Sigma}^K_{\alpha}(k,\omega)^{\mathrm{C}}$. In performing the integral of ω' in eq. (2.14), therefore, we rotate the integration path along the real axis into the imaginary axis counter-clockwise to avoid such poles considering an infinitesimal imaginary part in the non-interacting Green's function.[28,14] Then, we must remember to add contributions from a finite number of poles of the Green's function. The details of the calculations are shown in Appendix A.

The actual numerical calculation of the self-energy requires vast computational time. First, the polarization function given by eq. (2.9) involves the summation and

integration over wave vectors in the circumference n' and axis direction k', respectively, for all values of q and ω. Further, the self-energy requires the summation and integration over wave vectors (m', q) and the integration over ω'. Thus, the actual calculation of each self-energy requires double summations over the wave vector in the circumference direction and triple integrations over the wave vector in the axis direction and the frequency. The integration over q and ω' should actually be performed very carefully because the integrand has singularities at different points with various degrees.

Actually, only the use of eq. (2.25) makes the explicit determination of interaction effects on the band structure feasible. A self-consistent determination of the Green's function and the corresponding quasi-particle energy requires the calculation of the self-energy for all (k, ω) many times and is practically impossible for the present system without introducing further approximations. Besides, a self-consistent determination does not necessarily give more accurate results because corresponding vertex corrections should usually be considered for the consistency of the approximation.

3.2 Band gaps

Figure 2 gives the numerical results of the first and second band gaps for a semiconducting CN ($\nu = 1$) versus the effective strength of the Coulomb interaction. The first band means $n = 0$ in eq. (2.25) for the K and K' point and the second $n = 1$ for the K point or $n = -1$ for the K' point. When the Coulomb interaction is not strong, i.e., for $(e^2/\kappa L)/(2\pi\gamma/L) \lesssim 0.3$, the results in the static RPA are almost the same as those in the full dynamical approximation, showing that the static approximation is sufficient in this parameter range. Even in this weak coupling regime, the band gaps are considerably enhanced due to the Coulomb interaction. For $(e^2/\kappa L)/(2\pi\gamma/L) = 0.1$, for example, the first band gap with interaction is about 1.5 times as large as that without interaction. Furthermore, for $(e^2/\kappa L)/(2\pi\gamma/L) < 0.05$, the results in the Hartree-Fock approximation become equally valid.

3.3 Single-particle energy and effective mass

Figure 3 shows the dispersion relation of the single-particle energy of the first and second conduction bands measured from the Fermi level for $(e^2/\kappa L)/(2\pi\gamma/L) =$ 0.1, 0.2, and 0.5. Because of the particle-hole symmetry, only the conduction bands are shown in these figures. For each coupling constant, the Coulomb interaction generates nearly constant shifts to both bands in static and dynamical RPA. There exists little difference in both approximations for weak coupling, and the shift in dynamical RPA becomes a little smaller than that in the static case for larger coupling.

The constant energy shift is also supported by the fact that the Coulomb energy dependence of the effective mass m^* is rather small (at most 15 %) compared to that of the band gap as shown in Fig. 4. The dynamical effect on the effective mass along the axis direction is also quite small for $(e^2/\kappa L)/(2\pi\gamma/L) < 0.3$, while it becomes more apparent for $(e^2/\kappa L)/(2\pi\gamma/L) \sim 1$ than that on the band gaps. Away from weak-coupling regime, the dynamical RPA can cause positive shift to the effective mass, while the static RPA shows almost constant negative shift which is always smaller than that in the dynamical case. In the Hartree-Fock approximation the mass is considerably reduced with the increase of the interaction strength.

3.4 Diameter dependence

So far, we have considered only the fixed value of the cutoff energy $\varepsilon_c/(2\pi\gamma/L) = 5$. In this case the interaction parameter is independent of the CN diameter and therefore the band gap is inversely proportional to the circumference length L or the diameter $d = L/\pi$ even in the presence of interaction. Actually, however, a small dependence on the CN diameter d can appear through the cutoff energy ε_c. In fact, the cutoff should be chosen as $\varepsilon_c \sim 3\gamma_0$ corresponding to the π band width of the 2D graphite, giving $\varepsilon_c/(2\pi\gamma/L) \sim (\sqrt{3}/\pi)(L/a)$. Therefore, a dependence on the CN diameter d appears through this cutoff energy.

The band gaps shown in Fig. 5 are calculated for $\varepsilon_c/(2\pi\gamma/L) = 2.5$, 5, and 10 in the Hartree-Fock approximation and the dynamical RPA. We can see that the cut-off energy induces a small correction to the band gap that scales as $2\pi\gamma/L \propto 1/d$. The correction shows logarithmic increase with respect to ε_c, and this means that the band gap scaled by the inverse of the diameter contains a term that shows a logarithmic dependence on the diameter. In fact, as shown in Appendix B, it is analytically estimated that the band gaps have such a term as $\delta\Delta_n \propto (2\pi\gamma/L)\ln[\varepsilon_c/(2\pi\gamma/L)] \sim (2\pi\gamma/L)\ln(d/a)$ in both the Hartree-Fock approximation and the static RPA. The results given in Fig. 5 show the presence of such contributions in the dynamical RPA, too.

§4. Discussion

Figure 2 shows that the shift in the gap is almost independent of the band except in the Hartree-Fock approximation. Furthermore, the band gap is considerably enhanced due to the Coulomb interaction while the effective mass in the axis direction is slightly changed as shown in Figs. 2 and 4. Therefore, there exists a large difference in the interaction effect on the band gap and the effective mass. These facts show that the Coulomb interaction effects cannot be absorbed into a renormalization of the single band parameter γ. In the absence of interaction, the first and second band gaps become $4\pi\gamma/3L$ and $8\pi\gamma/3L$, respectively, and the corresponding effective masses are given by $2\pi\hbar^2/3L\gamma$ and $4\pi\hbar^2/3L\gamma$, respectively. Therefore, a renormalization of γ should give the fact that the ratio between the first and second gaps should remain the same and that the effective mass should also be reduced by the same amount as that of the band-gap enhancement.

The failure of the γ renormalization is quite possible because the Coulomb interaction is weaker than the typical band energy, i.e., $e^2/\kappa L \lesssim 2\pi\gamma/L$. In the weak-coupling regime, the interaction effect on the band gap can vary from that on the dispersion relation because they are likely to involve different energy scales. If we consider the strong interaction regime, $e^2/\kappa L \gg 2\pi\gamma/L$,

with a sufficiently large cutoff energy, the structure of the discrete energy bands will become less important. In this case electronic properties of the system will be similar to those in 2D graphite sheets and then interaction effects may be absorbed into a simple renormalization of γ. The present results are understood reasonably well in terms of a constant shift in the band gap together with a small renormalization of γ due to interaction effects.

In actual nanotubes, the coupling strength $(e^2/\kappa L)/(2\pi\gamma/L)$ is at most 0.35 as mentioned in the previous section. From Figs. 2, 3(a), 3(b), and 4, we can safely conclude that the dynamical screening effects are sufficiently weak both for band gaps and for effective mass and, therefore, that the static approximation is really satisfactory.

The logarithmic cutoff dependence obtained in the previous section shows that the band-gap enhancement increases slightly (logarithmically) with the increase of the CN diameter d if being scaled by $2\pi\gamma/L$. Previously, the diameter dependence of the band gap in a CN was investigated in various ways both from theoretical and experimental aspects.

Theoretically, for example, calculations of the band gaps were performed in a first-principles local-density approximation.[30] The result is that the first band gaps show almost $1/d$ dependence in the range of the diameter from about 0.7–2.6 nm and we cannot be certain whether they have a logarithmic correction on their $1/d$ dependence. The logarithmic dependence on the CN diameter comes from the (screened) nonlocal exchange term as shown in Appendix B and therefore it is doubtful that a logarithmic correction can appear in the local-density approximation where interaction effects are incorporated only in the form of a local exchange-correlation potential.

Experimentally, the first band gap was directly measured by scanning tunneling microscopy and spectroscopy.[15,16] In both refs. 15 and 16, the first band gaps measured for various CN's are consistent with the $1/d$ dependence. However, large error bars prevent verification of the deviation from the $1/d$ dependence.

Optical absorption spectra were measured in thin films of single-wall nanotubes and the optical gap displays slightly more rapid decrease than the $1/d$ scaling with increase of the CN diameter.[21] This is in contrast to our result in which the gap shows a slightly slower decrease than the $1/d$ dependence because of the presence of the logarithmic term. In the optical transition, however, excitons can play a crucial role[31,32,13] and we should actually study the diameter dependence of the exciton binding energy in order to make precise comparison between experiments and theory. Furthermore, effects of curvature may also be important for CN's with a small diameter ~ 1 nm.[33]

The exciton binding energy is larger for the second gap than the first due to larger effective mass, while the many-body shift of the gap is almost same for the first and second gap.[13] Therefore, it is possible to evaluate the Coulomb interaction parameter from the frequencies of those optical transitions. A comparison was made between experiments and theory for optical absorption spectra and, as a result, $(e^2/\kappa L)/(2\pi\gamma/L)$ was estimated to be about 0.05.[20] However, the dependence on the cutoff parameters was not studied carefully in ref. 13 and therefore there still remains some uncertainty in this value of the coupling strength. More detailed study on excitons and their cutoff dependence is required for better understanding of the optical spectra.

§5. Summary

In this paper, we have studied effects of the Coulomb interaction on the band structure of a semiconducting CN using a full dynamical random-phase approximation within an effective-mass scheme. The band gaps are strongly enhanced but effects on the effective mass are much smaller. As a consequence, interaction effects cannot be absorbed into a renormalization of a single band parameter γ. For the interaction parameter $(e^2/\kappa L)/(2\pi\gamma/L)$ appropriate in actual systems, the static approximation (screened Hartree-Fock approximation) has been shown to work sufficiently well. Furthermore, the band gaps with interaction have a small correction depending on the CN diameter, which can be estimated from the cutoff-energy dependence as $\delta\Delta_n \propto (\gamma/d)\ln(d/a)$.

Acknowledgments

We thank Mr. Tatsuya Yaguchi for a fruitful discussion. This work has been supported in part by Grants-in-Aid for COE (12CE2004 "Control of Electrons by Quantum Dot Structures and Its Application to Advanced Electronics") and Scientific Research from the Ministry of Education, Science and Culture, Japan.

Appendix A: Correlation Part of Self-Energy

In this appendix, we shall briefly explain the method of calculating the correlation term in the self-energy. In evaluating the contribution from the correlation term, we should change the contour C_1 along the real axis into C_2 along the imaginary axis in the complex ω' plane in eq. (2.14) in order to avoid the poles of $\varepsilon_{n-m}(q,\omega')$.[28,14] Figure 6 shows an example of singularities and two contours. The resulting self-energy consists of the contribution from the poles of the Green's function and that of the integral along the imaginary axis, i.e.,

$$\tilde{\Sigma}^K_{n+}(k,\varepsilon^K_{n+}(k))^{\rm C} = \tilde{\Sigma}^K_{n+}(k)^{\rm res} + \tilde{\Sigma}^K_{n+}(k)^{\rm line}. \qquad \text{(A1)}$$

The former is given by

$$\begin{aligned}&\tilde{\Sigma}^K_{n+}(k)^{\rm res}\\ &= \frac{1}{A}\sum_{m,q}\theta\big[\varepsilon^K_{n+}(k)-\varepsilon^K_{m+}(k+q)\big]F^{\nu K}_{n+,k;m+,k+q}\,v_{n-m}(q)\\ &\times\Big(\frac{1}{\varepsilon_{n-m}[q,\varepsilon^K_{m+}(k+q)-\varepsilon^K_{n+}(k)]}-1\Big)g_0[\varepsilon^K_{m+}(k+q)],\end{aligned} \qquad \text{(A2)}$$

where $\theta(t)$ is the step function defined by $\theta(t)=1$ for

$t>0$ and $\theta(t)=0$ for $t<0$. The latter is given by

$$\tilde{\Sigma}^K_{n+}(k)^{\rm line} = -\frac{1}{2\pi A}\int_{-\infty}^{\infty}{\rm d}\omega' \sum_{\beta,q}\frac{\varepsilon^K_{n+}(k)-\varepsilon^K_\beta(k+q)}{\omega'^2+[\varepsilon^K_{n+}(k)-\varepsilon^K_\beta(k+q)]^2} \times F^{\nu K}_{n+,k;\beta,k+q}\, v_{n-m}(q)\Big(\frac{1}{\varepsilon_{n-m}(q,{\rm i}\omega')}-1\Big)g_0[\varepsilon^K_\beta(k+q)]. \tag{A3}$$

The integration of ω' in eq. (A3) has a singularity at $\varepsilon^K_{n+}(k)-\varepsilon^K_\beta(k+q)=0$. We can avoid this singularity by replacing ω' with $\omega''=\omega'/(\varepsilon^K_{n+}(k)-\varepsilon^K_\beta(k+q))$.

Appendix B: Cutoff Dependence

Here, we shall discuss the dependence of the band gap Δ^K_n on the cutoff energy ε_c in the Hartree-Fock approximation. From eqs. (2.22) and (2.26), the enhancement of the band gap due to the Coulomb interaction can be expressed in the Hartree-Fock approximation as

$$\delta\Delta^K_n = \sum_{m,q}\frac{{\rm sgn}(n-\nu/3)\kappa_\nu(m)}{A\sqrt{\kappa_\nu(m)^2+q^2}}\, v_{n-m}(q) g_0\big[\gamma\sqrt{\kappa_\nu(m)^2+q^2}\big], \tag{B1}$$

where ${\rm sgn}(t)=1$ for $t>0$ and ${\rm sgn}(t)=-1$ for $t<0$. Since we consider the cutoff energy sufficiently large, we can replace the summation over m by an integral and have

$$\delta\Delta^K_n \sim \int{\rm d}m\int{\rm d}q\,\frac{e^2}{\kappa L}\frac{{\rm sgn}(n-\nu/3)}{\sqrt{(n-m)^2+q^2}}\frac{m-\nu/3}{\sqrt{(m-\nu/3)^2+q^2}} \times g_0\Big[\frac{2\pi\gamma}{L}\sqrt{(m-\nu/3)^2+q^2}\Big], \tag{B2}$$

where q is scaled by $2\pi/L$ and the summation can safely be replaced by the integral for large m and q. Further, we have used $v_{n-m}(q)\sim(e^2/\kappa)[(n-m)^2+q^2]^{-1/2}$, which is valid for large $|n-m|$ and $|q|$.

When n and $\nu/3$ are much smaller than m and q, the above becomes

$$\delta\Delta^K_n \sim \int{\rm d}m\int{\rm d}q\,\frac{e^2}{\kappa L}\frac{{\rm sgn}(n-\nu/3)}{m^2+q^2} \times\Big[\Big(\frac{m^2(n+\nu/3)}{m^2+q^2}-\frac{\nu}{3}\Big)g_0\Big(\frac{2\pi\gamma}{L}\sqrt{m^2+q^2}\Big) - \frac{2\pi\gamma\nu}{3L}\frac{m^2}{\sqrt{m^2+q^2}}\,g_0'\Big(\frac{2\pi\gamma}{L}\sqrt{m^2+q^2}\Big)\Big], \tag{B3}$$

where $g_0'(\varepsilon)=\partial g_0/\partial\varepsilon$. We can easily find that the second term including $g_0'(\varepsilon)$ in the bracket of the right hand side of eq. (B3) only gives contributions independent of ε_c, which will be ignored completely in the following. By introducing the polar coordinate (ε,θ) through $m=\varepsilon\cos\theta$ and $q=\varepsilon\sin\theta$, we have

$$\delta\Delta^K_n \sim \int_{n_{\rm min}}^{\varepsilon_c/(2\pi\gamma/L)}{\rm d}\varepsilon\int_0^{2\pi}{\rm d}\theta\,\frac{e^2}{\kappa L}\frac{{\rm sgn}(n-\nu/3)}{\varepsilon} \times\Big[\Big(n+\frac{\nu}{3}\Big)\cos^2\theta-\frac{\nu}{3}\Big] \sim \frac{\pi e^2}{\kappa L}\Big|n-\frac{\nu}{3}\Big|\,\ln\frac{\varepsilon_c}{(2\pi\gamma/L)n_{\rm min}}, \tag{B4}$$

where we have introduced an infrared cutoff $n_{\rm min}$, which should be chosen in such a way that the above approximations are valid for m and q satisfying $\varepsilon\equiv\sqrt{m^2+q^2}>n_{\rm min}$. Thus, the exchange contribution to the band gap contains a term which shows a logarithmic dependence on the cutoff energy.

Similarly, we can estimate the cutoff dependence in the static RPA. In this case, we only have to replace $v_{n-m}(q)$ by $v_{n-m}(q)/\varepsilon_{n-m}(q,0)$ in eq. (B1). Considering that static polarization function $P_{n-m}(q,0)$ can be approximated by that for a 2D graphite sheet for large m and q (for $\varepsilon>n_{\rm min}$), we have $P_{n-m}(q,0)\sim(\pi/2\gamma)\sqrt{(n-m)^2+q^2}$.[34] Apart from terms independent of ε_c, the resulting band gap in the static RPA becomes

$$\delta\Delta^K_n \sim \frac{\pi e^2}{\kappa L}\frac{|n-(\nu/3)|}{1+\pi^2(e^2/\kappa L)/(2\pi\gamma/L)}\ln\frac{\varepsilon_c}{(2\pi\gamma/L)n_{\rm min}}, \tag{B5}$$

which shows a similar logarithmic dependence although the coefficient is reduced by the screening effect.

References

1) S. Iijima: Nature (London) **354** (1991) 56.
2) N. Hamada, S. Sawada and A. Oshiyama: Phys. Rev. Lett. **68** (1992) 1579.
3) J. W. Mintmire, B. I. Dunlap and C. T. White: Phys. Rev. Lett. **68** (1992) 631.
4) R. Saito, M. Fujita, G. Dresselhaus and M. S. Dresselhaus: Phys. Rev. B **46** (1992) 1804; Appl. Phys. Lett. **60** (1992) 2204.
5) M. S. Dresselhaus, G. Dresselhaus and R. Saito: Phys. Rev. B **45** (1992) 6234.
6) R. A. Jishi, M. S. Dresselhaus and G. Dresselhaus: Phys. Rev. B **47** (1993) 16671.
7) K. Tanaka, K. Okahara, M. Okada and T. Yamabe: Chem. Phys. Lett. **191** (1992) 469.
8) Y. D. Gao and W. C. Herndon: Mol. Phys. **77** (1992) 585.
9) D. H. Robertson, D. W. Brenner and J. W. Mintmire: Phys. Rev. B **45** (1992) 12592.
10) C. T. White, D. C. Robertson and J. W. Mintmire: Phys. Rev. B **47** (1993) 5485.
11) H. Ajiki and T. Ando: J. Phys. Soc. Jpn. **62** (1993) 1255.
12) H. Ajiki and T. Ando: J. Phys. Soc. Jpn. **65** (1996) 505.
13) T. Ando: J. Phys. Soc. Jpn. **66** (1997) 1066.
14) L. Hedin: Phys. Rev. **139** (1965) A796; A. W. Overhauser: Phys. Rev. B **3** (1971) 1888; L. Hedin and S. Lundqvist: *Solid State Physics*, ed. F. Seitz, D. Turnbull and H. Ehrenreich (Academic, New York, 1969) Vol. 23, p. 1.
15) J. W. Wildoer, L. C. Venema, A. G. Rinzler, R. E. Smalley and C. Dekker: Nature (London) **391** (1998) 59.
16) T. W. Odom, J. -L. Huang, P. Kim and C. M. Lieber: Nature **391** (1998) 62.
17) See, for example, A. G. S. Filho, A. Jorio, G. Dresselhaus, M. S. Dresselhaus, R. Saito, A. K. Swan, M. S. Ünlü, B. B. Goldberg, J. H. Hafner, C. M. Lieber and M. A. Pimenta: Phys. Rev. B **65** (2002) 035404 and references cited therein.
18) H. Ajiki and T. Ando: Physica B **201** (1994) 349; Jpn. J. Appl. Phys. Suppl. **34-1** (1995) 107.
19) H. Kataura, Y. Kumazawa, Y. Maniwa, I. Umezu, S. Suzuki, Y. Ohtsuka and Y. Achiba: Synth. Met.

103 (1999) 2555.
20) M. Ichida, S. Mizuno, Y. Tani, Y. Saito and A. Nakamura: J. Phys. Soc. Jpn. **68** (1999) 3131.
21) M. Ichida, S. Mizuno, Y. Saito, H. Kataura, Y. Achiba and A. Nakamura: Phys. Rev. B **65** (2002) 241407.
22) J. C. Slonczewski and P. R. Weiss: Phys. Rev. **109** (1958) 272.
23) L. Wang, P. S. Davids, A. Saxena and A. R. Bishop: Phys. Rev. B **46** (1992) 7175.
24) M. F. Lin and K. W. -K. Shung: Phys. Rev. B **48** (1993) 5567.
25) M. F. Lin and K. W. -K. Shung: Phys. Rev. B **47** (1993) 6617.
26) O. Sato, Y. Tanaka, M. Kobayashi and A. Hasegawa: Phys. Rev. B **48** (1993) 1947.
27) P. J. Lin-Chung and A. K. Rajagopal: Phys. Rev. B **49** (1994) 8454.
28) T. M. Rice: Ann. Phys. (N.Y.) **31** (1965) 100.
29) D. F. Du Bois: Ann. Phys. (N.Y.) **7** (1959) 174.
30) J. W. Mintmire and C. T. White: Carbon **33** (1995) 893.
31) R. Loudon: Am. J. Phys. **27** (1959) 649.
32) R. J. Elliot and R. Loudon: J. Phys. Chem. Solids **8** (1959) 382; **15** (1960) 196.
33) X. Blase, L. X. Benedict, E. L. Shirley and S. G. Louie: Phys. Rev. Lett. **72** (1994) 1878.
34) J. González, F. Guinea, and M. A. H. Vozmediano: Phys. Rev. B **59** (1999) R2474.

Figure Captions

Fig. 1 (a) The diagram of the self-energy in the random-phase approximation. (b) The diagram of the full polarization function.

Fig. 2 Calculated band gaps in a semiconducting CN as a function of the effective strength of the Coulomb interaction $(e^2/\kappa L)/(2\pi\gamma/L)$. The first band gap corresponds to that of $n=0$ for both K and K' points and the second $n=1$ for the K point or $n=-1$ for the K' point.

Fig. 3 Calculated single-particle energy levels for the conduction band in a semiconducting CN. (a) $(e^2/\kappa L)/(2\pi\gamma/L)=0.1$, (b) 0.2, and (c) 0.5.

Fig. 4 The effective mass for the first and second band in a semiconducting CN versus the effective strength of the Coulomb interaction, estimated from the single-particle energy of each band.

Fig. 5 The cutoff-energy dependence of the first and second band gap in a semiconducting CN. The band gaps are calculated for $\varepsilon_c/(2\pi\gamma/L)=2.5$, 5, and 10.

Fig. 6 The contours C_1 and C_2 in the complex ω' plane. The Green's function in the integrand gives poles denoted by crosses and the dielectric function is singular along the dotted lines. The integral along C_1 is equal to that along C_2 plus the contribution of the pole at $-\omega+\varepsilon_{m+}(k+q)-\mathrm{i}\delta$.

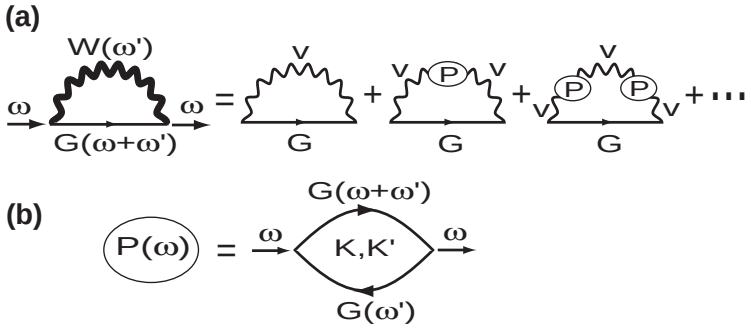

Fig. 1

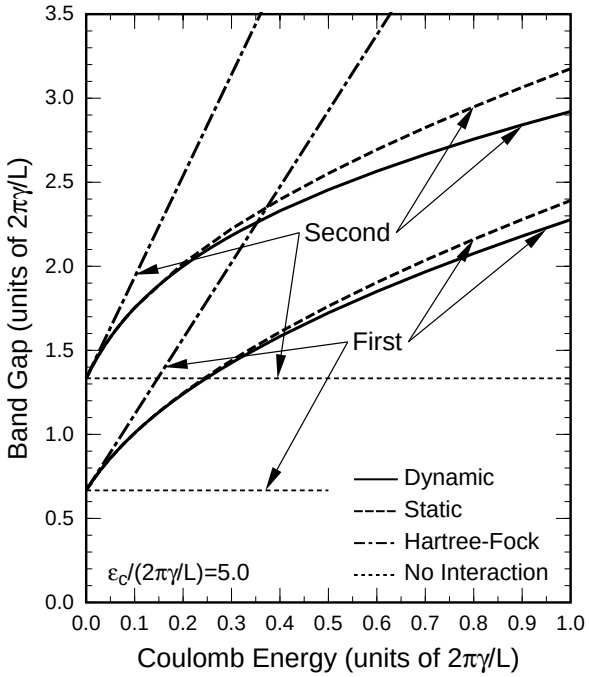

Fig. 2

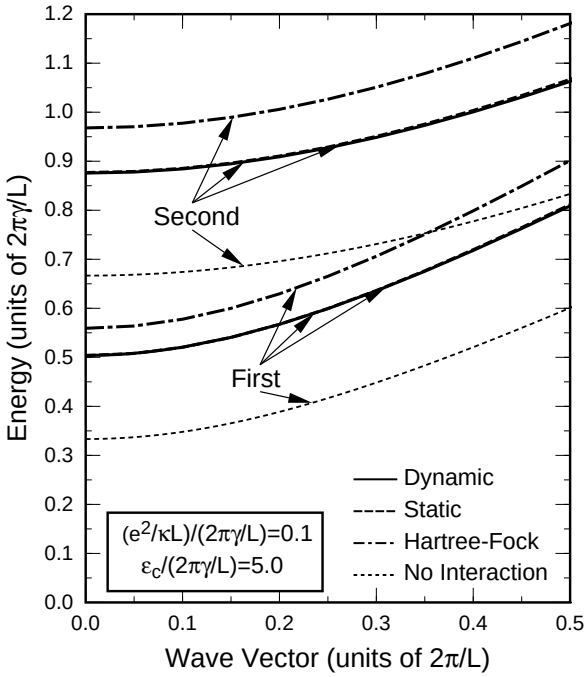

Fig. 3 (a)

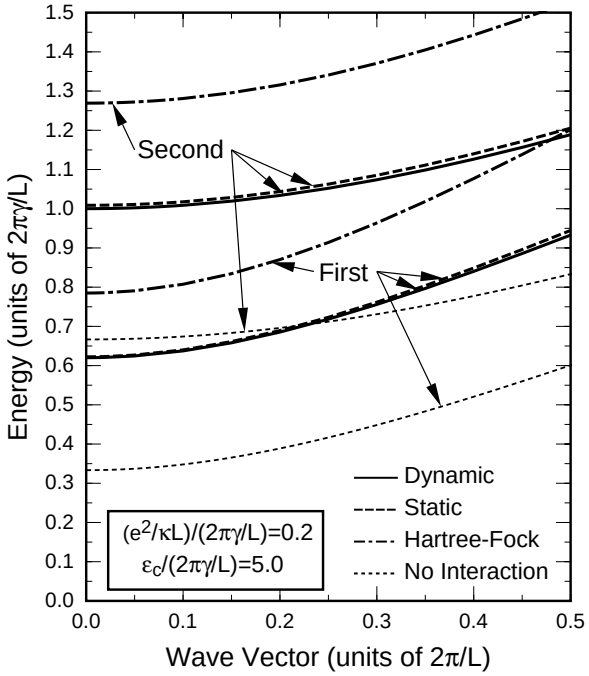

Fig. 3 (b)

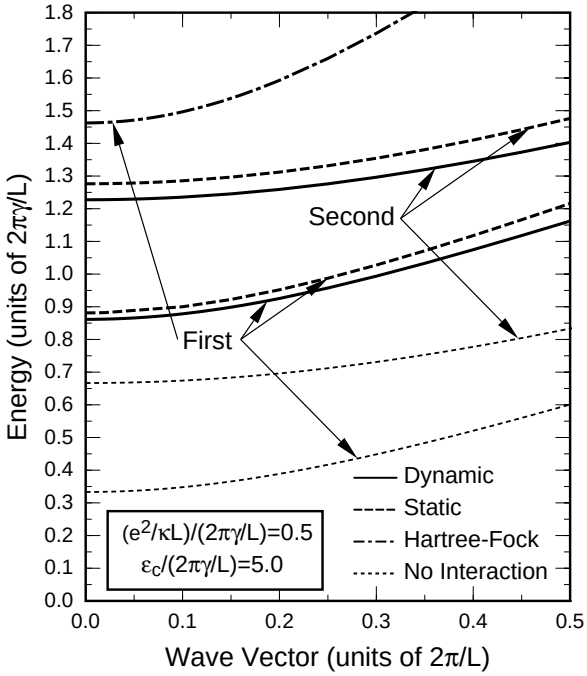

Fig. 3 (c)

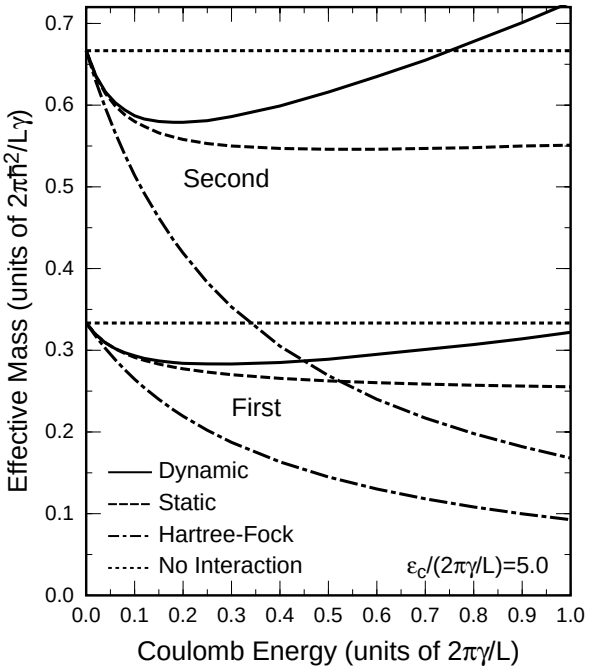

Fig. 4

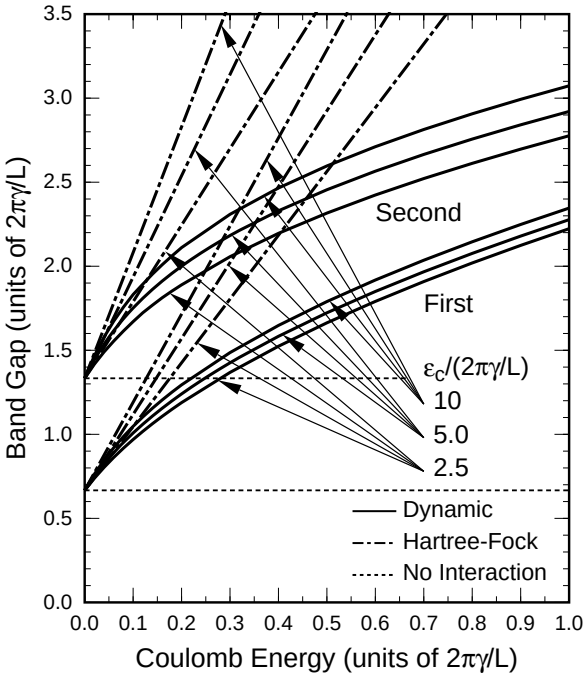

Fig. 5

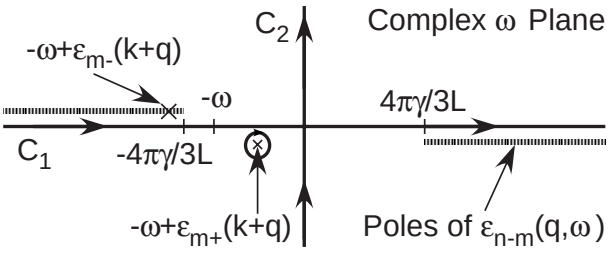

Fig. 6